Jomo Kenyatta University of Agriculture and Technology

College of Engineering and Technology

School of Mechanical, Materials, and Manufacturing Engineering

Department of Mechatronic Engineering

Design and Fabrication of a Dual Recovery System for the N4 Rocket (FYP-20-1)

INTERIM REPORT

Ian Kiptoo (ENM221-0067/2019)

Kennedy Mwendwa (ENM221-0199/2019)

Supervisor

Dr. Shohei Aoki

August 2024

Declaration

We hereby declare that the work contained in this report is original; researched and documented by the undersigned students. It has not been used or presented elsewhere in any form for award of any academic qualification or otherwise. Any material obtained from other parties have been duly acknowledged. We have ensured that no violation of copyright or intellectual property rights have been committed.

1. Ian Kiptoo

   Signature.....Date.....

2. Kennedy Mwendwa

   Signature.....Date.....

Approved by supervisors:

1. Dr.Shohei Aoki

   Signature.....Date.....

Abstract

In high-power rocketry, recovery systems are essential for ensuring safe descent and reuse. Traditional single-parachute systems are insufficient for high-altitude flights, as they lead to excessive drift and recovery challenges. This project focuses on developing a dual recovery system for the N4 high-power rocket. The system deploys two parachutes at different stages of the descent: a drogue parachute deploys at the highest point of flight to stabilize and slow the rocket's initial descent without causing excessive drift, while a main parachute deploys at a lower altitude to further slow the rocket for a controlled, safe landing near the launch site. The avionics bay, which doubles as a structural coupler, houses the flight computer responsible for the timing and management of the ejection charges. These charges, along with shear pins, ensure the correct sequence of parachute deployment. The system is engineered to withstand the forces of descent and achieve safe terminal velocities. With the design now complete, the next phase is to construct and test the system in real-world conditions.

Contents

List of Figures

List of Tables

1 Introduction

The dual deployment parachute recovery system has become an essential technique in high-power rocketry, providing enhanced safety and precision during descent. Initially, rocket recovery relied on single parachute systems, which often resulted in uncontrolled, hard landings that could damage both the rocket and its surroundings[1, 2]. In the 1980s, amateur rocketry groups began experimenting with dual deployment to address these issues, aiming to improve recovery accuracy and minimize drift caused by winds during descent. This innovation was driven by the need for safer landings, especially as rockets became more powerful and valuable.[1, 2]

The dual deployment system involves two parachutes: a drogue chute and a main chute, each deployed at different stages of descent to achieve controlled landings [1, 2]. The drogue chute deploys at apogee to stabilize the rocket and slow its descent without arresting it completely, preventing excessive tumbling [3]. Later, as the rocket nears the ground, the main parachute deploys to provide a gentle, controlled landing near the launch point [4]. This technique became widely adopted in the 1990s, especially within high-power rocketry, due to its effectiveness in ensuring safe and predictable recoveries.

Our project focuses on designing, implementing, and validating a dual deployment system, with the goal of ensuring reliable recovery and reducing drift, which is critical for maintaining safety and efficiency in high-power rocket operations [5].

1.1 Problem Statement:

In high-power rocketry, deploying the main parachute at a high altitude apogee results in excessive drift and a significantly slower descent. Consequently, the rocket often lands much further away from the launch point than desired. This extended drift makes tracking and recovering the rocket particularly challenging and time-consuming, especially when the landing site is in rough or inaccessible terrain. The increased distance and difficulty in recovery not only add to the operational complexity but also heighten the risk of losing valuable rocket components.

1.2 Objectives

1.2.1 Main Objective:

To design and fabricate a dual deployment parachute recovery system for the N4 rocket.

1.2.2 Specific Objectives:

The specific objectives of this project are as follows:

1. To design and fabricate the mechanical structure of the dual event ejection mechanism including the main and the drogue parachute.
2. To develop a fully functional flight computer with electronic circuitry, incorporating sensors for altitude, acceleration, position, orientation, and a communication module to the base station.
3. To develop a state machine using a filtering algorithm to detect apogee and determine the precise moments for drogue and main parachute deployment.
4. To integrate all the components into a functional dual recovery system.

1.3 Scope

The scope of this project encompasses the design and fabrication of a dual event ejection mechanism, which includes creating both the mechanical structure and the main and drogue parachutes. Additionally, the project involves developing a fully functional flight computer with integrated electronic circuitry and sensors for altitude, acceleration, position, and orientation, alongside a communication module for real-time data transmission to a base station. A key component of the project is the development of a state machine using a filtering algorithm to accurately detect the rocket's apogee and determine the precise moments for deploying the drogue and main parachutes. Finally, all these components will be integrated into a cohesive and operational dual recovery system, ensuring the rocket's safe and controlled descent.

1.4 Justification:

Recovering rockets after high-altitude ejections presents significant challenges due to wind drift, which can cause rockets to land far from the intended recovery zone, complicating and prolonging the recovery process. This can be particularly problematic in rough or inaccessible terrains, making it difficult to locate and retrieve the rocket promptly. By implementing a dual-recovery system, which employs both a drogue and a main parachute, we can substantially mitigate these issues. The drogue parachute deploys at apogee, stabilizing and slowing the descent without fully arresting it, while the main parachute deploys at a lower altitude, ensuring a slower, controlled descent and reducing horizontal drift. This system enhances safety by minimizing the risk of damage during landing and increases efficiency by ensuring the rocket lands closer to the launch point. Consequently, the dual-recovery system not only facilitates quicker and more predictable recoveries but also boosts the overall success rate of missions by reducing the likelihood of loss or damage to the rocket.

2 Literature Review

2.1 History of Dual Recovery Systems

The history of dual recovery systems in rocketry began in the late 20th century, driven by the need for safer and more controlled recoveries in high-power and experimental rocketry. Initially, single parachute deployments were used, but they proved inadequate for high-altitude flights due to high descent speeds and significant drift.The figure below shows a single parachute deployment system used by Estes model rockets.

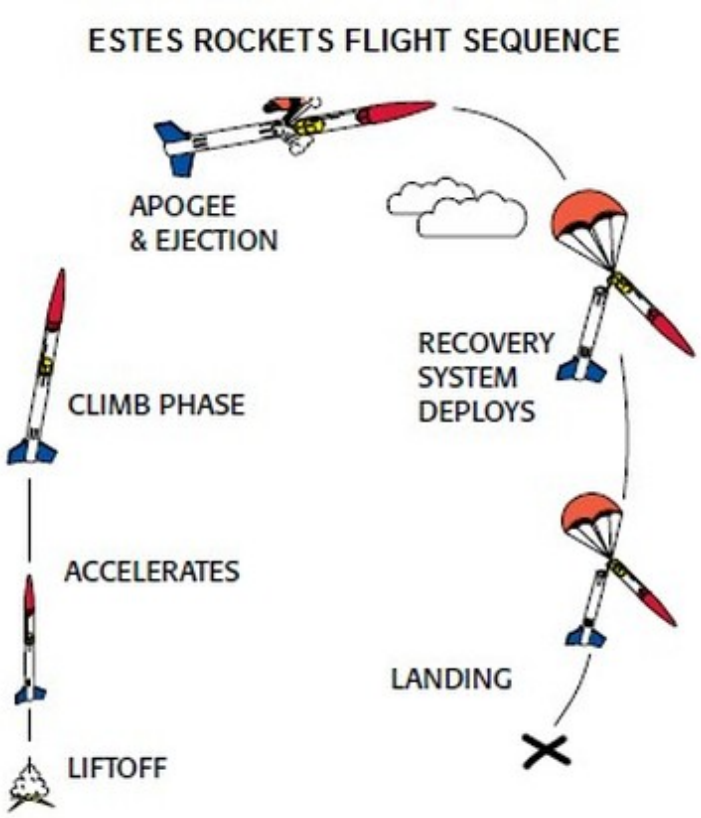

Figure 2.1: A high-power rocket utilizing a single recovery system.

In the 1980s and 1990s, pioneers in the field, supported by organizations like the Tripoli Rocketry Association and the National Association of Rocketry, started developing two-stage parachute systems [6]. The advent of reliable altimeters and flight computers allowed precise control over the timing of drogue and main parachute deployments, reducing descent speeds and improving landing accuracy [7].

By the 1990s and early 2000s, dual recovery systems had gained widespread acceptance thanks to advances in affordable electronics and growing recognition of their benefits in competitions and high-altitude flights [8]. Modern iterations have integrated advanced sensors, GPS technology, and real-time data logging, enhancing their accuracy and reliability [9]. Today, dual event ejection systems are standard in high-power rocketry, ensuring safe and predictable recoveries and supporting ongoing innovation in the field [10].

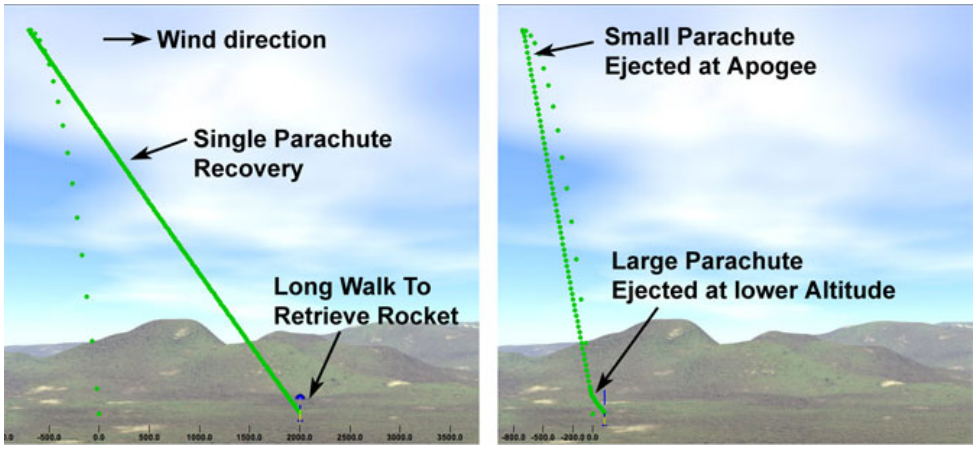

Figure 2.2: Comparison of drift between a single and a dual recovery system

2.2 Operation Sequence

The operation sequence in dual recovery systems involves multiple stages to ensure a controlled descent. In rockets developed by BPS Space and the TRA, the sequence begins at apogee, where an onboard altimeter, such as the PerfectFlite Stratologger CF, detects the highest point of the rocket's flight. At this point, a signal is sent to deploy the drogue

parachute. The drogue parachute stabilizes the rocket and slows its descent, reducing terminal velocity to a manageable level and preventing excessive drift caused by high-altitude winds [11].

As the rocket continues its descent, a second altitude threshold is reached, typically between 500 to 1,000 feet above ground level. The altimeter or a separate barometric sensor, such as the Altus Metrum TeleMega, triggers the deployment of the main parachute. The main parachute significantly increases drag, further slowing the descent to ensure a soft landing. This two-stage recovery process reduces the risk of damage to the rocket and its payload, allowing for safe retrieval and reuse [12].

Figure 2.3: A high-power rocket utilizing a dual recovery system.

2.3 Comparison of Parachute Types

Table 2.1: Types of parachutes and their characteristics

Parachute Type	**Drag Coefficient (Cd)**	**Descent Stability**	**Ease of Fabrication**	**Image**
Hemispherical	1.3 - 1.5	High, tends to be stable with minimal oscillation	Moderate, relatively simple pattern and assembly	
Circular	0.75 - 1.2	Moderate, can oscillate if not reefed or vented	Simple, basic design and straightforward assembly	
Elliptical	1.0 - 1.3	High, more stable descent due to shape	Complex, requires precise cutting and sewing	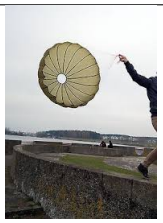
Toroidal	0.8 - 1.0	High, excellent stability due to aerodynamic shape	Complex, involves intricate design and assembly	

Table 2.1 compares parachute types, emphasizing the trade-offs between stability, drag efficiency, and fabrication complexity. Hemispherical and elliptical parachutes provide high stability, but elliptical designs are more complex. Circular parachutes are simpler but may lack stability. Toroidal parachutes offer excellent stability but are the most intricate to fabricate. The choice of parachute depends on balancing performance needs with ease of construction.

2.3.1 Parachute Design and Sizing

Parachute size is determined by the mass of the rocket, desired descent rate, and drag characteristics of the parachute. The calculation is a two-step process. First, the area,A,of the parachute is calculated using equation 2.1[13]

$$A = \frac{2mg}{\rho v_T^2 C_D} \tag{2.1}$$

where

- m = mass of the rocket,
- v_T = desired terminal velocity,
- C_D = drag coefficient of the parachute,
- $\rho = 1.22$ kg/m^3 = air density at sea level at 15°C,
- $g = 9.807$ m/s^2 = acceleration due to gravity.

The diameter is then calculated from the surface area based on the shape:- For hexagonal parachutes, the diameter,D, can be calculated as shown in equation (2.2), while for square parachutes, the length of each side,L, is calculated using equation (2.3). For all other parachutes, the shape is assumed to be circular and the diameter is calculated using equation (2.4).[14]

$$D = \sqrt{\frac{2A}{\sqrt{3}}} \tag{2.2}$$

$$L = \sqrt{A} \tag{2.3}$$

$$D = \sqrt{\frac{4A}{\pi}} \tag{2.4}$$

2.3.2 Materials Used in Parachute Fabrication

The selection of materials for parachute fabrication is critical to ensure reliability and performance. The common materials used are summarized in table 2.2[15]

Table 2.2: Comparison of Materials

Material	**Advantages**	**Disadvantages**
Ripstop Nylon	- Lightweight. - High tear resistance. - Low porosity, reducing air leakage.	- Can degrade under prolonged UV exposure. - Less flexible compared to other fabrics.
Silk	- Very lightweight and strong. - Smooth texture reduces air drag.	- Prone to UV damage. - Higher cost compared to synthetic fabrics.
Kevlar	- High strength-to-weight ratio. - Excellent thermal stability.	- Expensive material. - Difficult to sew and fabricate.

2.4 Ejection Mechanisms

Ejection mechanisms in rocketry are designed to deploy recovery devices, such as parachutes, at specific points during the rocket's descent. They typically use small explosive charges or pressurized systems to forcibly separate sections of the rocket, allowing the parachutes to deploy and slow the rocket's descent for a safe landing.

2.4.1 Pyrotechnic Charges

Pyrotechnic charges are widely used for their reliability and ability to function under extreme conditions. These charges consist of small explosive devices that, when ignited,

rapidly expand gases to forcefully eject the parachute. The explosive charges commonly used are black powder and crimson powder. Black powder, also known as gunpowder, is a well-known propellant composed of potassium nitrate (KNO_3), charcoal (C), and sulfur (S). The simplified chemical reaction for the combustion of black powder is:

$$2KNO_3 + 3C + S \rightarrow K_2CO_3 + CO_2 + N_2 + SO_2 \tag{2.5}$$

Figure 2.4: Diagram of pyrotechnic ejection sequence

The gases produced by the combustion process rapidly expand, exerting pressure on the

surrounding components, resulting in the deployment of the parachute [16]. The pressure required for ejection is determined by the desired force, or alternatively, the force can be set by specifying the desired pressure. This relationship is given by equation(2.6).

$$P = \frac{F}{\pi \left(\frac{D}{2}\right)^2} \tag{2.6}$$

where:

- F = Desired force
- D = Body tube diameter

Once the desired pressure P is known, the amount of black powder required can be calculated using equation(2.7).

$$m = \frac{PV}{R_c T g} \tag{2.7}$$

where:

- P = Pressure calculated from the previous equation
- V = Volume of the chamber to be pressurized
- $R_c = 12.1579 \, \frac{m}{K}$ (combustion gas constant for FFFFg black powder)
- $T = 1739 \, K$ (combustion gas temperature)
- $g = 9.807 \, \frac{m}{s^2}$ (acceleration due to gravity) [17]

2.4.2 Spring-based Systems

Spring-based ejection systems,shown in figure 2.5, offer a mechanical alternative to pyrotechnic charges. These systems rely on the potential energy stored in compressed springs to deploy parachutes. When triggered, the springs release their energy, pushing out the parachute. This method is particularly useful in environments where pyrotechnics are not allowed or are deemed unsafe. Spring-based systems are more complex to design but offer reliable performance with fewer safety concerns [18].

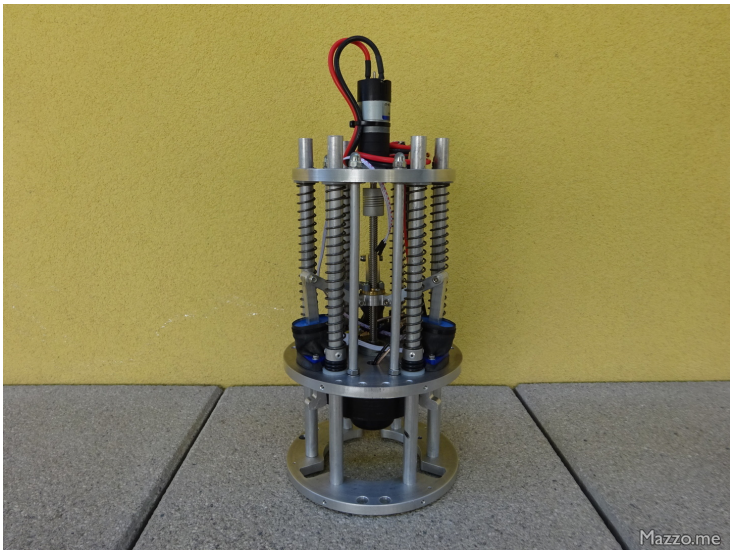

Figure 2.5: Image of a spring based ejection system Image source

2.5 Avionics and Sensors

Avionics in dual recovery systems include altimeters, barometric pressure sensors, accelerometers, and gyroscopes. These components work together to determine the rocket's position, speed, and altitude. The altimeter is the primary sensor, typically measuring changes in atmospheric pressure to determine altitude. Accelerometers measure the rocket's acceleration during ascent and descent, while gyroscopes provide data on orientation and stability [7].

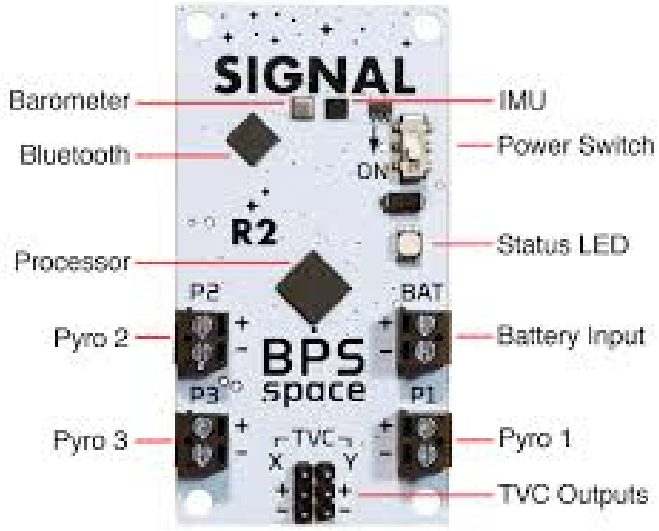

Figure 2.6: Example of avionics system in a rocket. Image source

2.5.1 Flight Software Implementation

The flight software in dual recovery systems is essential for processing avionics data and managing parachute deployments. Typically written in C++ or Python, this software handles several critical tasks:

- **Apogee Detection:** Algorithms process sensor data to accurately determine the rocket's apogee, ensuring timely deployment of recovery systems [19].
- **Ejection Control:** The software controls the deployment sequence of parachutes based on apogee detection and flight parameters [20].
- **Data Logging and Telemetry:** It logs flight data and transmits it to ground stations, providing real-time monitoring and post-flight analysis [21].
- **Safety Checks:** Redundancy and safety checks are implemented to minimize the risk of failure and ensure reliable operation [22].

The software used by organizations like the Tripoli Rocketry Association (TRA) exemplifies these principles by integrating multiple sensor inputs to enhance accuracy and reliability [23].

2.6 Filtering Algorithms

In high-power rocketry, accurately estimating a rocket's position, velocity, and other dynamic states in real time is essential for recovery. Due to the noisy nature of sensor data and the complex, nonlinear behavior of the rocket's flight, advanced filtering algorithms are required to extract meaningful estimates from noisy measurements. This section examines three key filtering techniques commonly used in high-power rocketry: the 2D Kalman Filter, the Extended Kalman Filter (EKF), and the Particle Filter (PF). The 2D Kalman Filter is well-suited for linear flight dynamics but struggles with the nonlinearities typical in rocket trajectories. The EKF addresses this by linearizing the system around current estimates, making it more applicable to the non-linear environment of a rocket's flight. For even more complex scenarios involving highly nonlinear dynamics and non-Gaussian noise, the Particle Filter offers a more robust solution by approximating the rocket's state using a set of weighted particles. These filters play a crucial role in ensuring the accuracy and reliability of onboard state estimation throughout the rocket's flight phases.

2.6.1 2D Kalman Filter

The 2D Kalman Filter extends the traditional Kalman Filter to estimate the state of a system in two dimensions, such as position and velocity, based on noisy measurements. It iteratively updates the state estimate and the associated uncertainty by incorporating new measurements. The filter follows three key equations:

$$\hat{x}_k = \hat{x}_{k-1} + K_k \left(z_k - H\hat{x}_{k-1} \right) \tag{2.8}$$

This equation updates the state estimate $\hat{x}_k$, where $\hat{x}_{k-1}$ is the previous estimate, z_k is the new measurement, and H is the measurement matrix that relates the state to the measurement. The term K_k represents the Kalman Gain, which determines how much the measurement influences the update.

$$P_k = (I - K_k H) P_{k-1} \tag{2.9}$$

This equation updates the uncertainty (covariance matrix) P_k, accounting for how much the new measurement reduces the overall uncertainty. I is the identity matrix, and K_k is the Kalman Gain, which reduces the uncertainty based on the reliability of the measurement.

$$K_k = \frac{P_{k-1} H^T}{H P_{k-1} H^T + R} \tag{2.10}$$

The Kalman Gain K_k is calculated based on the previous uncertainty P_{k-1}, the measurement matrix H, and the measurement noise covariance R. It balances the weight given to the new measurement against the current state estimate's uncertainty.

The 2D Kalman Filter differs from the 1D version by estimating two interrelated state variables (e.g., position and velocity), instead of one, and updating the state and uncertainty in both dimensions simultaneously. This allows it to handle more complex systems like those in high-power rocketry, where both position and velocity change dynamically during flight.

2.6.2 Extended Kalman Filter (EKF)

The Extended Kalman Filter is an extension of the 2D Kalman Filter that handles nonlinear systems by linearizing them around the current estimate. The EKF updates the state estimate using:

$$\hat{x}_k = \hat{x}_{k-1} + K_k \left(z_k - h(\hat{x}_{k-1}) \right) \tag{2.11}$$

$$P_k = (I - K_k H_k) P_{k-1} \tag{2.12}$$

$$K_k = \frac{P_{k-1}H_k^T}{H_k P_{k-1} H_k^T + R} \tag{2.13}$$

where: - $h(\hat{x}_{k-1})$ = nonlinear measurement function - H_k = Jacobian matrix of $h(\hat{x}_{k-1})$

2.6.3 Particle Filter (PF)

The Particle Filter estimates the state of a system using a set of particles, each representing a possible state. It updates the particles and their associated weights based on the likelihood of the measurement given each particle's state. The state estimate is computed as the weighted average of the particles.

$$\hat{x}_k = \sum_{i=1}^{N} w_k^{(i)} x_k^{(i)} \tag{2.14}$$

where: - $x_k^{(i)}$ = state of the i-th particle at time k - $w_k^{(i)}$ = weight of the i-th particle at time k - N = number of particles

2.6.4 Key Differences

- **System Type:** The 2D Kalman Filter is best suited for linear systems, while the EKF can handle nonlinear systems by linearizing them. The Particle Filter can handle highly nonlinear and non-Gaussian systems without the need for linearization.
- **Complexity:** The 2D Kalman Filter and EKF are computationally efficient due to their recursive nature. The Particle Filter is more computationally intensive as it involves simulating multiple particles and resampling them at each step. [24]
- **Estimation Accuracy:** The Particle Filter provides more accurate estimates in complex scenarios with non-linearities and non-Gaussian noise, while the EKF may struggle with significant non-linearities. The 2D Kalman Filter is precise for linear systems but not suitable for non-linear systems.

2.6.5 Telemetry

Table 2.3 presents a comparison of different communication modules available for high-power rocketry.

Table 2.3: Comparison of communication modules for telemetry in amateur rocketry

Parameter	**Digi XBee-PRO 900HP**	**LoRa**	**Wi-Fi (ESP32)**
Bandwidth	200 kbps	37.5 kbps	54 Mbps (802.11g), 150 Mbps (802.11n)
Range	Up to 45 km (line of sight)	Up to 15-20 km (line of sight)	Up to 200 meters (line of sight)
Power Consumption	250 mW (transmit), 0.5 mW (sleep)	10-50 mW (transmit), ¡1 mW (sleep)	500 mW (transmit), 50 mW (idle), 2 mW (sleep)

BPS Space uses the 915 MHz LoRa transceiver for telemetry communication, which enables long-range, low-power data transmission. This module transmits data on altitude, speed, and parachute deployment status to ground control stations. Additionally, the use of a u-blox NEO-M8N GPS module provides real-time tracking of the rocket's location [24].

TRA rockets often use the XBee Pro 900HP for wireless data links, which supports robust communication over long distances. Real-time tracking capabilities are also provided by GPS modules, such as the u-blox NEO-M8N. These systems transmit continuous data streams on flight dynamics and recovery status, crucial for real-time decision-making and post-flight analysis [25].

2.7 Research Gaps

Despite the advancements in dual recovery systems for high-power amateur rockets, there are still several areas for improvement:

Table 2.4: Comparison between Nakuja N3.5 group's implementation and research gaps

Nakuja N3.5 Implementation	**Research Gap**
The group used a one-dimensional Kalman filter for altitude estimation.	A 2D Kalman filter can combine both accelerometer and BMP data, providing more accurate and precise altitude estimation.
The avionics bay was used solely as a housing for electrical components.	Dual use of the avionics bay as a structural coupler can optimize space and reduce overall weight.
No real-time adaptive algorithms were implemented to handle unexpected flight anomalies.	Implementing real-time adaptive algorithms can improve flight reliability by adjusting for unexpected conditions.
Unreliable onboard data logging capabilities for post-flight analysis.	Enhanced onboard data logging can provide comprehensive post-flight data for more detailed analysis.

3 Methodology

3.1 Mechanical Design

The approach began with the parachute design, where considerations were made for the size and type of parachutes needed to achieve desired descent rates and stability.

The next step involved determining the appropriate shear pin diameters, which are critical for ensuring the parachutes deploy at the right moment. Eye bolts were then designed for the shock cords, ensuring they could handle the required loads and secure the shock cords properly.

Finally, calculations were made for the coupler screws used to assemble the avionics bay, ensuring they were strong enough to maintain the integrity of the structure while being easy to assemble and disassemble.

3.1.1 Parachute Design Considerations

Figure 3.1 shows the components of a parachute subsystem, the gores are the individual subsections which are sewn together to form the whole parachute. The small opening at the top is the vent which is designed to minimise oscillation of the parachute during descent. The extension lines, also known as shock cords, connects the parachute to the load which in our case is the rocket.The size of the parachute determines the descent velocity of the system,given all other parameters remain constant. The mass of the rocket is equal to the difference between the mass of the rocket assembly and the mass of the fuel. The total mass of the assembly from simulations was found to be 26kg. The mass of the fuel was 6kg. Therefore the total mass during recovery after all the fuel was used up was found to be $m = 20$kg. The following are the important parameters that were used in designing the parachutes:

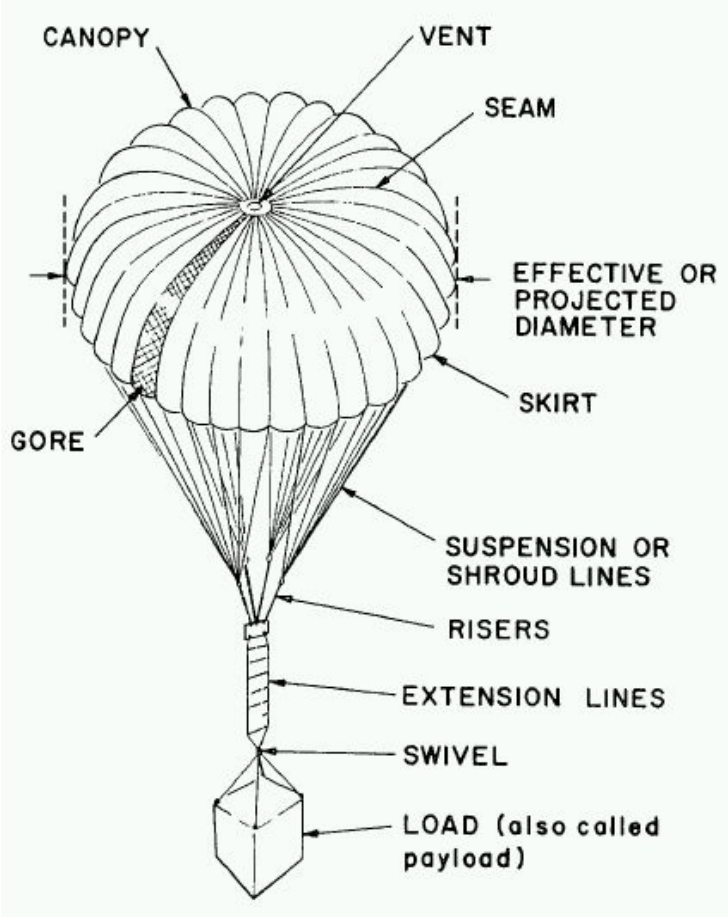

Figure 3.1: Components of a parachute system Image source

- Drag coefficient,Cd,which is a dimensionless quantity used to quantify the resistance or drag of the parachute in a fluid environment.It is approximately 1.54 for hemispherical parachutes.

The parachutes causes the rocket to descend at a particular velocity called a terminal velocity. The Spaceport America Cup challenge recommends a terminal velocity of between 20 and 50m/s for drogue parachutes and a terminal velocity of below 10m/s for the main parachute.

- Terminal velocity V_t for drogue parachute was selected as 21 m/s.
- Terminal velocity $V_t$for the main parachute was selected as 5.5 m/s

- $m = 20$ kg (mass of the rocket)
- $C_d = 1.54$ (drag coefficient for hemispherical parachutes)
- $g = 9.8$ m/s^2 (gravitational acceleration)
- $\rho = 1.225$ kg/m^3 (air density)

The parameters above were used in equation (3.1) to find the parachute area,A.

$$A = \frac{2mg}{\rho C_d V_t^2} \tag{3.1}$$

The nominal area of the main parachute was calculated as $6.87\,\mathrm{m}^2$.
The nominal area of the drogue parachute was calculated as $0.47\,\mathrm{m}^2$.

The hemispherical shape was selected for the main and drogue parachute due to its ease of fabrication. From the parachute areas calculated in equation (3.1) and using equation (2.4). The diameters of the parachutes were calculated to be:

The nominal diameter of the main parachute was calculated as $2.96\,\mathrm{m}$.
The nominal diameter of the drogue parachute was calculated as $0.77\,\mathrm{m}$.

The number of gores for the main parachute is usually taken as 8 and that of the drogue taken as 4.

The spill hole or apex vent area, as per Rocketman Enterprises, is taken as 1% of the canopy area to minimize parachute oscillation, was calculated as:

$$\text{Drogue chute spill hole area} = 0.047\,\mathrm{m}^2$$

The diameter of the spill hole from equation (2.4) was:

$$D_2 = 0.24\,\mathrm{m}$$

Main parachute spill hole area $= 0.069\,\mathrm{m}^2$

The diameter of the spill hole from equation (2.4) was:

$D_2 = 0.30\,\mathrm{m}$

Shock Cord Design

Following the parachute design, the shock cord was designed to connect the parachutes to the rocket and withstand the forces experienced during deployment.

The parachute opening shock was estimated using the Pflanz Method, which combines empirical and semi-empirical models to calculate the peak force generated during parachute deployment. This force depends on several key parameters, including rocket mass, deployment velocity, parachute size, and atmospheric conditions.

The Pflanz Method was used to estimate the parachute opening shock force with equation (3.2) shown below:

$$F_x = (S \cdot C_D)_p \cdot q \cdot C_x \cdot X_1 \tag{3.2}$$

where F_x represents the parachute opening shock force, $(S \cdot C_D)_p$ is the product of the parachute surface area and drag coefficient, q is the dynamic pressure, C_x is the empirical opening force coefficient, and X_1 is the force reduction factor based on the ballistic parameter A. All the key parameters were obtained as follows:

Rocket Mass

The rocket's mass m is a critical factor influencing the total gravitational force W_t, which contributes to the opening shock force:

$$W_t = m \cdot g \tag{3.3}$$

For this analysis, the rocket's mass was 20 kg, resulting in a gravitational force $W_t = 196.2\,\mathrm{N}$.

Deployment velocity and Dynamic Pressure

The deployment velocity v_t is another factor which influences the dynamic pressure q as part of the Pflanz Method.The dynamic pressure was obtained using equation (3.4):

$$q = \frac{1}{2} \cdot \rho \cdot v_t^2 \tag{3.4}$$

For this project, the velocity at deployment of the main parachute was $v_t = 21\,\mathrm{m/s}$,which is the terminal velocity of the drogue parachute, leading to a dynamic pressure $q = 270.11\,\mathrm{Pa}$.The air density was taken as $\rho = 1.225\,\mathrm{kg/m^3}$

Parachute Size and Drag Coefficient

The effective drag area $(S \cdot C_D)_p$ was obtained by multiplying the surface area of the parachute S and the drag coefficient C_D using equation (3.5):

$$S = \pi \cdot \left(\frac{D}{2}\right)^2 \tag{3.5}$$

Given that the parachute diameter D was 2.9 meters and $C_D = 1.54$, the calculated effective drag area was $(S \cdot C_D)_p = 10.16\,\mathrm{m^2}$.

Inflation Time and Canopy Fill Constant n

The inflation time t_f of the parachute was calculated using the canopy fill constant $n = 1.5$ and parachute diameter $D_0 = 2.9\,\mathrm{m}$ using equation (3.6) as:

$$t_f = \frac{n \cdot D_0}{v_t} \tag{3.6}$$

The inflation time was determined to be $t_f = 0.207\,\mathrm{seconds}$.

Ballistic Parameter A

The ballistic parameter A was calculated using equation (3.7) as:

$$A = \frac{2 \cdot W_t}{(S \cdot C_D)_p \cdot \rho \cdot g \cdot v_1 \cdot t_f} \tag{3.7}$$

For the given parameters, the ballistic parameter A was calculated to be approximately 0.74.

Force Reduction Factor X_1

The force reduction factor X_1 was determined from empirical data for the calculated value of $A = 0.74$. From the corresponding charts, $X_1 = 0.99$.

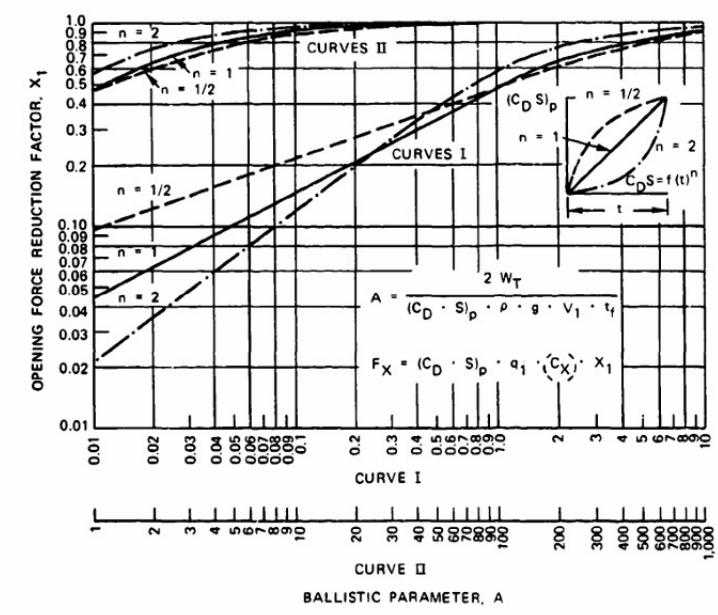

Figure 3.2: Components of a parachute system and force reduction factor

Finally, using the Pflanz Method equation, the parachute opening shock force F_x was calculated yielding the result:

$$F_x \approx 4618\,\text{N}$$

The value of C_x was derived from the chart shown in figure 3.3.

TABLE 5-1. Solid Textile Parachutes.

TYPE	CONSTRUCTED SHAPE PLAN	CONSTRUCTED SHAPE PROFILE	$\frac{D_c}{D_o}$	INFLATED SHAPE $\frac{D_p}{D_o}$	DRAG COEF C_{D_o} RANGE	OPENING FORCE COEF C_X (INF MASS)	AVERAGE ANGLE OF OSCILLATION, DEGREES	GENERAL APPLICATION
FLAT CIRCULAR			1.00	0.67 TO 0.70	0.75 TO 0.80	~1.7	±10 TO ±40	DESCENT, OBSOLETE
CONICAL			0.93 TO 0.95	0.70	0.75 TO 0.90	~1.8	±10 TO ±30	DESCENT, M < 0.5
BICONICAL			0.90 TO 0.95	0.70	0.75 TO 0.92	~1.8	±10 TO ±30	DESCENT, M < 0.5
TRICONICAL POLYCONICAL			0.90 TO 0.95	0.70	0.80 TO 0.96	~1.8	±10 TO ±20	DESCENT, M < 0.5
EXTENDED SKIRT 10% FLAT		$0.1\,D_c$	0.86	0.66 TO 0.70	0.78 TO 0.87	~1.4	±10 TO ±15	DESCENT, M < 0.5
EXTENDED SKIRT 14.3% FULL		$0.143\,D_c$	0.81 TO 0.85	0.66 TO 0.70	0.75 TO 0.90	~1.4	±10 TO ±15	DESCENT, M < 0.5
HEMISPHERICAL			0.71	0.66	0.62 TO 0.77	~1.6	±10 TO ±15	DESCENT, M < 0.5, OBSOLETE
GUIDE SURFACE (RIBBED)			0.63	0.62	0.28 TO 0.42	~1.2	0 TO ±2	STABILIZATION, DROGUE, 0.1 < M < 1.5
GUIDE SURFACE (RIBLESS)			0.66	0.63	0.30 TO 0.34	~1.4	0 TO ±3	PILOT, DROGUE, 0.1 < M < 1.5
ANNULAR			1.04	0.94	0.85 TO 0.95	~1.4	<±6	DESCENT, M < 0.5
CROSS			1.15 TO 1.19	0.65 TO 0.72	0.60 TO 0.85	1.1 TO 1.2	0 TO ±3	DESCENT, DECELERATION

Figure 3.3: Empirical opening force coefficient chart

The estimated parachute opening shock force for a 20 kg rocket deploying a 2.9-meter diameter parachute at 21 m/s was approximately 4618 N. This estimation, derived using the Pflanz Method, provided a conservative result which serves as a safety margin when compared to other methods such as Ludtke's method or the Moment Impulse Theorem.

3.1.2 Shear Pin Diameter Calculation

Shear pins are mechanical components used to secure parts in place while allowing them to separate under a specified force. They are designed to shear off when a predetermined load is exceeded, thus protecting other components from damage. In our design, the predetermined load for failure was chosen as 285N and 380N for the drogue and main parachute shear pins respectively.The number of shear pins to be used for the drogue and main parachutes were also selected intuitively as 4 and 3 respectively. This section outlines the calculations used to determine the appropriate diameter of shear pins for both the main and drogue parachutes.

Design Considerations for Shear Pins

- Material: PLA. PLA was chosen because of its relatively low shear strength hence could shear off with less force and also result in a bigger shear pin diameter which would be easy to fabricate.
- Shear Strength: $\tau = 26.77$ MPa
- Main Parachute Shear Force: $F_{\text{shear}} = 285$ N, Number of Pins: $n = 3$
- Drogue Parachute Shear Force: $F_{\text{shear}} = 380$ N, Number of Pins: $n = 4$

The shear force to be withstood by the pins was given as:

$$P_s = \frac{\pi}{4} \times d^2 \times \tau \times n \tag{3.8}$$

Making d the subject of the formula and using the parameters provided above, the diameters for both the main and drogue parachutes were found to be approximately 2.126mm say 3mm using equation (3.8)

3.1.3 Ejection Charge Calculations

Following the shock cord design, the next step was to calculate the ejection charges necessary to deploy the parachutes effectively.The amount of force required to break the shear pins and push out the parachute determined the amount of black powder charge to be used.The distance the parachutes are to be thrown out also was selected intuitively as 4m and 2m.The force to overcome shear pins were taken from the shear pin discussion. The distance the parachutes were to be pushed by the ejection force is the distance from the bottom of the parachute bay to the nearest vent hole where the pressure producing the ejection force would be relieved. The diameter of the chamber was obtained from the N3.5 air-frame team.The height of the chamber was estimated using existing chamber allocations from the N3.5 recovery team.All these parameters are provided in table 3.1.

Design Considerations

Table 3.1: Design Considerations for Ejection Charges

Parameter	**Main Parachute**	**Drogue Chute**
Mass of parachute, m_p	0.3 kg	0.3kg
Mass of nosecone, m_n	0.35 kg	0.35kg
Total mass, m	0.65 kg	4.78 kg
Distance to be thrown up by ejection force, h	4 m	2 m
Force to overcome shear pins, F_{sp}	285 N	380 N
Distance to push the parachute, d	0.2 m	0.2 m
Safety factor, sf	1.2	1.2
Diameter of chamber, D	0.1 m	0.1 m
Height of chamber, h_c	0.4 m	0.15 m
Gas constant for FFF black powder, R_c	265 J/(kg·K)	265 J/(kg·K)
Temperature, T	1739 K	1739 K
Acceleration due to gravity, g	9.81 m/s^2	9.81 m/s^2

Calculations

The potential energy required to eject the parachutes was calculated using equation (3.9):

$$PE = mgh \tag{3.9}$$

Using equation (3.9), the potential energy required to push out the main and the drogue parachutes to the required distances were found to be 25.5J and 93.7J respectively.

The force required to push the parachute was determined by dividing the potential energy by the distance over which it is applied:

$$F_p = \frac{PE}{d} \tag{3.10}$$

Using equation (3.10), the amount of force to push out the main and drogue parachutes were found to be 127.53 and 468.26N

The total force required to eject each parachute was calculated by adding the force to push the parachute and the force needed to overcome the shear pins. Moreover, a safety factor of 1.2 was applied to the resultant forces.Therefore, the forces required to eject the main and drogue parachutes were obtained as 495N and 1017N respectively.

The pressure needed in the chamber to achieve the required force was computed using the chamber's cross-sectional area,which was cylindrical in shape,using following equation:

$$A = \pi \left(\frac{D}{2}\right)^2 \tag{3.11}$$

The pressure required to provide the ejection force for the main parachute was calculated as 63101Pa while that required for the drogue parachute was found to be 129617Pa using equation (3.11).

The volume of the chamber was calculated to be used in determining the mass of black powder to be used using equation (3.12).

$$V_{\text{main}} = \pi \times \left(\frac{D}{2}\right)^2 \times h_c \tag{3.12}$$

From the dimensions provided in Table 3.1, the volume of the main chamber was obtained as $0.003\,\text{m}^3$ and that of the drogue chamber as $0.002\,\text{m}^3$.

Finally, the mass of the ejection powder required was determined using the pressure, volume, and properties of the gas:

$$m = \frac{P \times V}{R_c \times T \times g} \tag{3.13}$$

Equation (3.13) yielded the mass of charge to eject both the main and drogue parachute as approximately 1 gram each.

3.1.4 Design Calculations for Eye Bolt

The eye bolt is the component on to which the shock cord is tied so that it attaches the parachute to the rocket.The eye bolt was designed to withstand the shock load without failure. The following calculations were performed to determine the appropriate nominal diameter of the eye bolt,given that the shock load is reduced by a factor of 5 using the flexible shock cord.The allowable stress for the eye bolt was selected as 100Mpa to minimise its deformation.

Design Considerations:

- Load Reduction Factor: 0.7
- Shock load: 470 kg
- Allowable Stress allowed for the bolt: $\sigma = 100$ MPa
- Acceleration due to Gravity: $g = 9.81$ m/s^2

First, the load in kilograms was converted to Newtons then divided by the load reduction factor yielding a load of 3186.8N:

The nominal bolt diameter was calculated using equation (3.14):

$$P = \frac{\pi}{4} d_c^2 \times \sigma \tag{3.14}$$

where:

- P is the load in Newtons
- $\sigma$is the allowable stress in pascals

Rearranging the equation and solving for d, the diameter of the eye bolt was obtained as 6.36mm, the nearest dimension for the bolt was then selected as 8mm.

3.1.5 Bulkhead Screws Design

Bulkhead screws are used to secure the avionics bay to the airframe and the number of screws used need to be selected based on the shear stress they exert on the airframe. The following calculations were performed to ensure the screws could handle the shear stresses as well as prevent damage to the airframe.

Design Considerations:

- Material: Stainless steel due to its high shear strength hence allows us to work with smaller diameter screws
- Shear Strength: 65% of UTS, where UTS = 505 MPa
- Selected Screw Diameter,d = 5 mm
- Number of screws,n = 6
- Shear Force: $P_s = 3186.8\,\mathrm{N}$

Using The shear stress τ was calculated using equation (3.8):

- $P_s = 3186.8\,\mathrm{N}$ is the shear force
- $d = 5\,\mathrm{mm}$ is the screw diameter
- $n = 6$ is the number of screws

Rearranging to solve for τ,the calculated shear stress was obtained as:

$$\tau = 27.05\,\text{MPa}$$

This shear stress value was compared with the material's shear strength(44.8Mpa) to ensure it would not shear off.

3.2 Electrical Design

3.2.1 Flight Computer

The following table provides the power requirements for all the circuitry components used in the system, as well as the power calculations for each component. This includes both the operational and total power consumption across different voltage rails.

Component	**Voltage (V)**	**Current (A)**	**Power (W)**
ESP32 (NodeMCU)	5.0	0.160	0.8
BMP180	3.3	0.000005	0.0000165
MPU-6050	3.3	0.0039	0.01287
LORA Module	3.3	0.120	0.396
NEO-6M GPS Module	5.0	0.067	0.335
Nichrome Wire Igniters (2x)	14.8	2.0 (each)	59.2
Total (3.3V components)	3.3	0.123905	0.4088865
Total Input Power (5V)	5.0	0.227	1.135
Total Input Power (14.8V)	14.8	4.0	59.2

Table 3.2: Power Requirements of the Circuit Components

Total Power Requirement:

$$\text{Total Power (5V Rail)} = 0.8\,\text{W} + 0.335\,\text{W} = 1.135\,\text{W}$$

$$\text{Total Power (3.3V Rail)} = 0.0000165\,\text{W} + 0.01287\,\text{W} + 0.396\,\text{W} = 0.4088865\,\text{W}$$

$$\text{Total Power (14.8V Rail)} = 59.2\,\text{W}$$

$$\text{Total Power Requirement} = 1.135\,\text{W} + 0.4088865\,\text{W} + 59.2\,\text{W}$$

$$\text{Total Power Requirement} \approx 60.74\,\text{W}$$

3.2.2 Telemetry

The project required the transmission of sensor data upto 3km in altitude from an MPU6050, a GPS module, and a BMP sensor. To ensure effective communication, the data was organized into a structured format and transmitted at a frequency of 10 times per second.

The data structure was designed as follows:

- **MPU6050:** 6 axes of data (3 accelerometers + 3 gyroscopes) each at 2 bytes, totaling 12 bytes.
- **GPS Module:** Coordinates (latitude and longitude) at 4 bytes each, totaling 8 bytes.
- **BMP Sensor:** Temperature and pressure, each at 2 bytes, totaling 4 bytes.

Combining these, the total data payload per transmission was:

$$\text{Total Payload} = 12\ \text{bytes(MPU6050)} + 8\ \text{bytes(GPS)} + 4\ \text{bytes(BMP)} = 24\ \text{bytes}$$

Given that the data was to be transmitted 10 times per second, the required bandwidth was calculated as follows:

$$\text{Bandwidth} = \text{Total Payload} \times \text{Transmission Frequency}$$

$$\text{Bandwidth} = 24 \text{ bytes} \times 10 \text{ Hz} = 240 \text{ bytes/sec}$$

To convert this to bits per second:

$$\text{Bandwidth} = 240 \text{ bytes/sec} \times 8 \text{ bits/byte} = 1920 \text{ bits/sec or } 1.92 \text{ kbps}$$

LoRa offers bandwidths of up to 27 kbps, and since the required data rate is 1.92 kbps,LoRa satisfies the data transmission bandwidth requirement.Moreover, LoRa offers a line of sight range of 15-20km therefore LoRa satisfies the transmission range requirement to be selected as the communication module for the task.

4 Results and Discussion

4.1 Drogue Parachute

The design and calculations indicated that a canopy area of approximately 0.471 m^2 was required to achieve the desired terminal velocity of 21 m/s. The calculated diameter of the parachute canopy was 77.4 cm, with a corresponding circumference of 2.43 m. The chosen number of gores was 8, and the spill hole area was 0.047 m^2. These parameters ensured that the drogue parachute effectively slowed the rocket and stabilized it before the deployment of the main parachute.

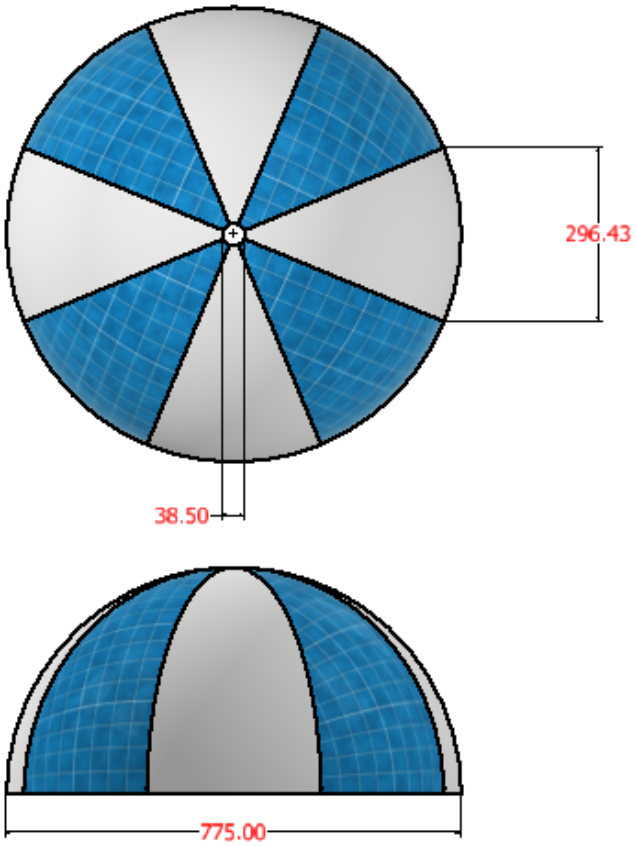

Figure 4.1: drogue chute

4.2 Main Parachute

For the main parachute, the required canopy area was determined to be 6.869 m^2 to achieve a terminal velocity of 5.5 m/s. The diameter of the main canopy was calculated to be 2.957 m with a circumference of 9.293 m. The parachute design included 20 gores, and the spill hole area was 0.069 m^2. These specifications aimed at ensuring a soft and controlled landing by significantly reducing the rocket's descent speed.

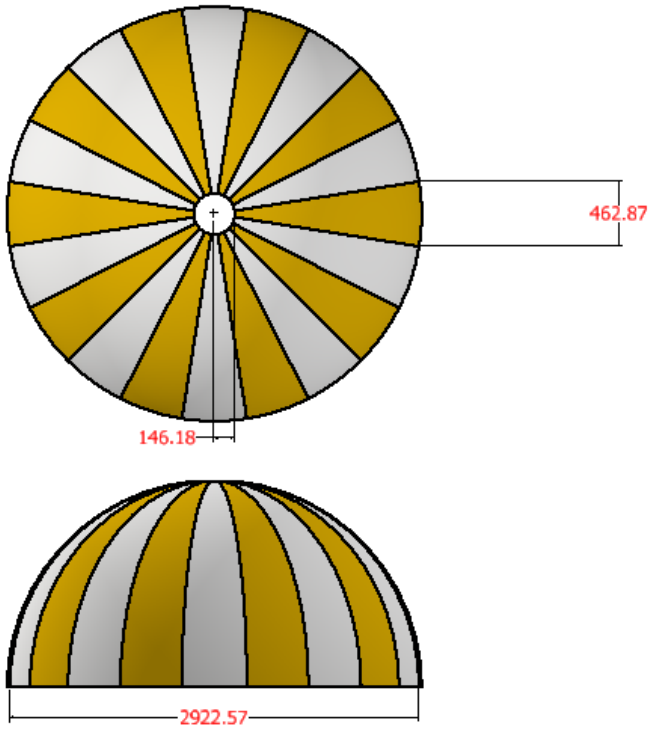

Figure 4.2: main chute

4.3 Shear Pins

The shear pin diameters for both the drogue and main parachutes were calculated based on the required shear forces and material strength. For the main parachute, the diameter was approximately 2.126 mm, while for the drogue parachute, it was the same, 2.126 mm. These diameters ensured that the pins could withstand the forces during deployment without premature failure and were capable of shearing off at the designated loads to

allow parachute deployment.

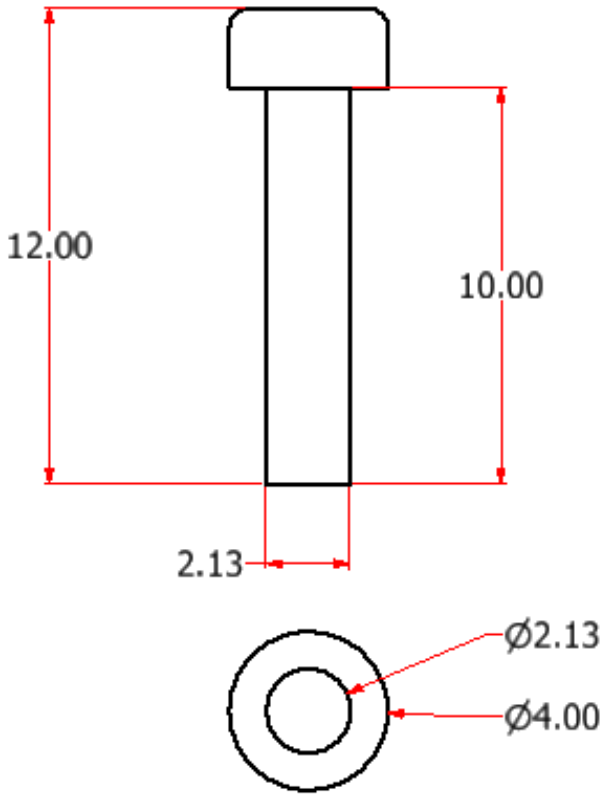

Figure 4.3: drogue chute

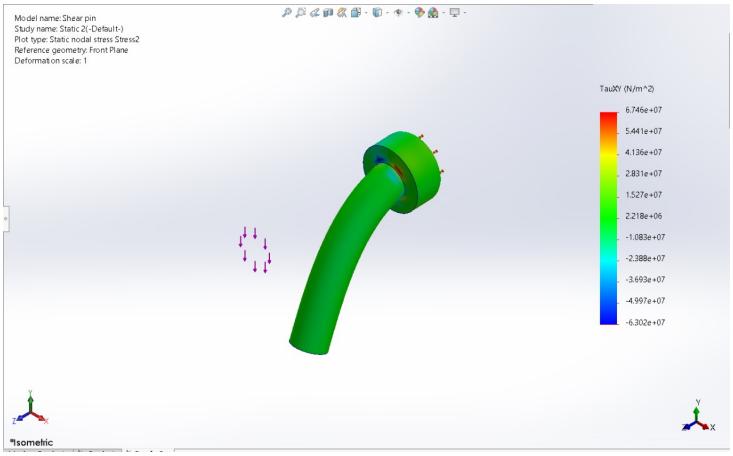

Figure 4.4: drogue chute

4.4 Avionics Bay

The avionics bay assembly, consists of several key components that ensure the structural integrity and functionality of the system. The **bulkheads** (Item 1) are positioned at the top and bottom, providing protection and enclosure for the avionics section. **Eye bolts (M6 DIN580)** (Item 2) are located at the top, facilitating secure attachment to other sections of the rocket. The **charge holder** (Item 3) houses the ejection charge, which is crucial for parachute deployment during recovery. The **avionics bay lid** (Item 4) covers the electronics compartment, safeguarding the internal components. **Threaded rods** (Item 5) run through the entire assembly, keeping the structure intact, while **DIN 6340-6.4 washers** (Item 6) and **hexagon nuts (ISO 4034 - M6)** (Item 7) ensure a tight and secure fit of the components. **Support rods** (Item 8) add stability, and the **bay protector** (Item 9) shields the avionics from external damage. Finally, **DIN 967 - M5 x 20 screws** (Item 10) are used to fasten various parts of the assembly together. This well-constructed system houses the electronics safely and allows for proper integration into the rocket's design.

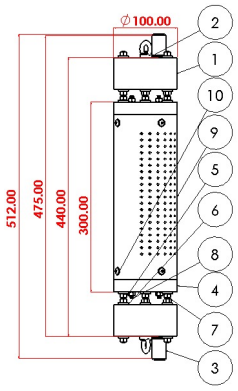

ITEM NO.	PART NUMBER	DESCRIPTION	QTY.
1	bulkhead		2
2	Eye bolt M6 DIN580		2
3	charge_holder		2
4	avionicsbaylid		2
5	threaded rod		6
6	DIN 6340-6.4		18
7	Hexagon Nut ISO 4034 - M6 - N		24
8	support rods		2
9	bay protector		1
10	DIN 967 - M5 x 20 - Z --- 18.4N		8

Figure 4.5: avionics bay parts list

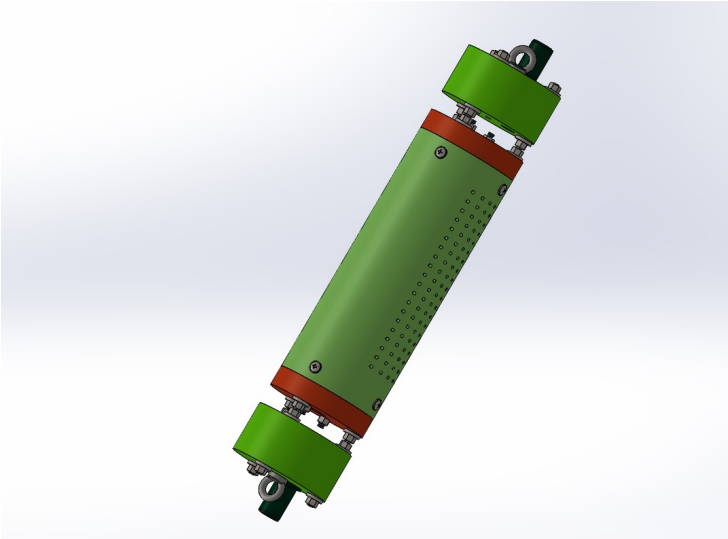

Figure 4.6: avionics bay model

4.5 Shock Cord

Using equation (3.2) the Opening force was calculated to be 4618N which translates to approximately 470.7kg.Table 4.1 shows the commonly used materials that are used in fabrication of the shock cords. Since a charge ejection deployment method had been selected, the high temperatures necessitated the use of a kevlar shock cord as the primary material for shock cord fabrication. Table 4.2 shows the thickness and widths of available shock cords and their corresponding breaking weights.From the calculated value of opening shock, the 15.875mm wide kevlar shock cord can withstand the opening shock of 470.7kg. hence it was selected.

4.6 Eye Bolt

The eye bolt was designed to handle significant loads, with a calculated diameter of approximately 6.36 mm. Considering practical availability, an 8 mm diameter was selected. This eye bolt was essential for securely attaching the shock cords and needed to endure the shock loads during deployment. The load reduction factor used ensured that the bolt remained within safe operational limits under expected forces.

Table 4.1: Shock Cord Material Selection

Section	**Material**	**Purpose**
Lower (50mm)	Kevlar	To protect the tubular nylon cord from high temperatures of ejection charge
Upper (8000mm)	Tubular Nylon	To absorb the opening shock from destroying the canopy

Table 4.2: Selection of shock cord width

Thickness	**Width**	**Breaking Weight**
0.08” (2.032mm)	5/8” (15.875mm)	1500lbs (680kg)
	1.25” (31.75mm)	3200lbs (1450kg)

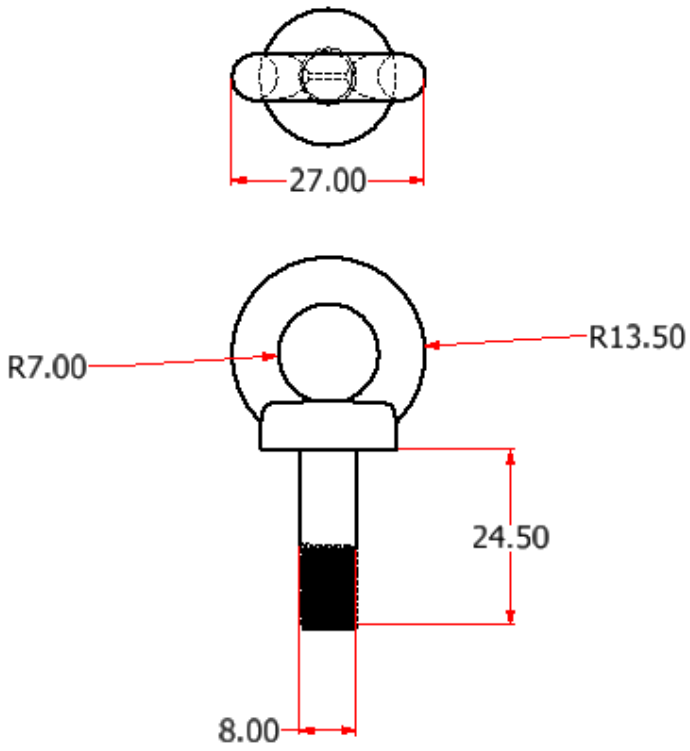

Figure 4.7: drogue chute

4.7 Ejection Charge

The ejection charge calculations for both the main and drogue parachutes involved determining the required pressure and mass of ejection powder. For the main parachute, a total force of 495.036 N with a safety factor was determined, translating into a required ejection powder mass of approximately 1 g. For the drogue parachute, the required force was 1017.917 N, and the mass of the ejection powder was about 0.930 g. These calculations ensured that the parachutes would deploy effectively and reliably.

4.8 Telemetry and Flight Computer

Lora was selected as the data transmission module as it was capable of long range communication coupled with enough bandwith to handle the data being transmitted by the flight computer at a data rate of 1.92Kbps. Its low power consumption propery was an added advantage.

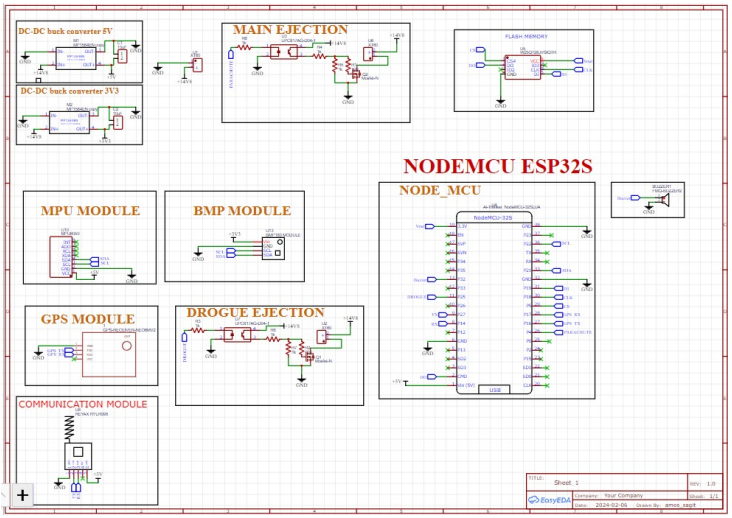

Figure 4.8: Flight Computer Circuitry

4.9 Control Flowchart

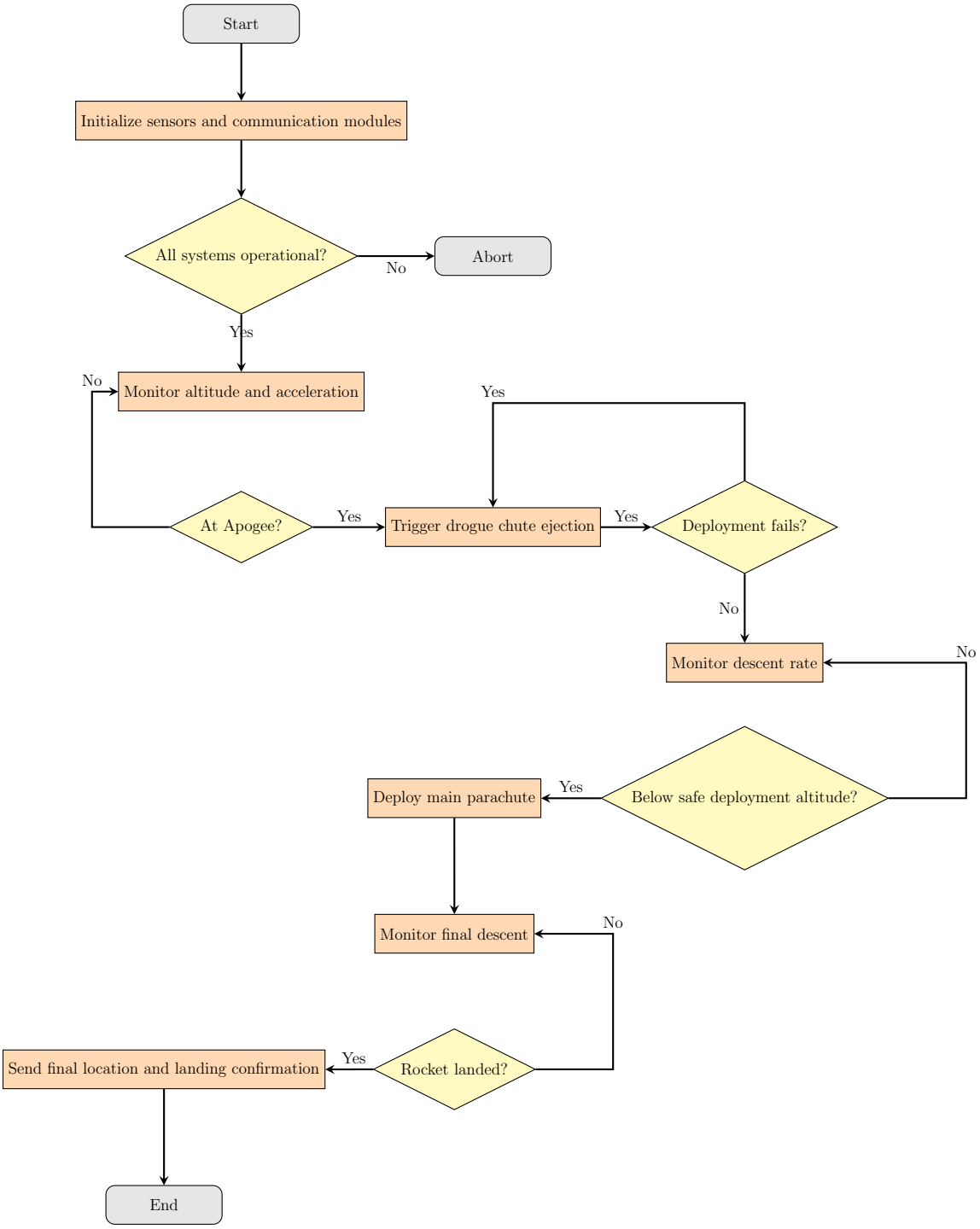

The dual recovery system for a high-speed powered rocket begins by initiating the sensors and communication module to monitor the rocket's status. It then checks if all systems are operational; if not, the process is aborted. If the systems are functioning

properly, the rocket's altitude and acceleration are monitored. Upon reaching apogee, the highest point in its flight, the drogue chute is deployed to slow the rocket's descent. The system checks whether the deployment was successful. If the drogue chute fails to deploy, the system monitors the descent, otherwise, it continues to check the descent rate. As the rocket descends, the system determines if it has dropped below a safe altitude for deploying the main parachute. If the altitude is safe, the main parachute is deployed to slow the rocket further for final descent. Throughout the descent, the system checks for a safe landing. Once the rocket lands, the system sends the final location and landing confirmation, marking the end of the process.

5 Summary, Conclusion, and Future Work

The first phase of this project focused on designing a dual recovery ejection mechanism for the N4 high-power rocket, incorporating a 3D-printed avionics bay and machined bulkheads. The avionics bay, designed to house the control electronics, is powered by a 14.8V battery. MOSFET transistors are employed to activate the igniters at precise moments, while voltage regulation for the sensors and microprocessor is managed by buck converters. The ejection mechanism is controlled by a state machine algorithm, with sensor data filtered using a Kalman filter.

The recovery system utilizes nylon shear pins for controlled separation and a hemispherical drogue and main parachute for reliable performance and ease of fabrication. An electronic switch is included to arm the ejection mechanism, ensuring safety during handling.

With the design now complete, the next steps involve fabricating the components based on the finalized specifications. This includes 3D printing the avionics bay and coupler, machining the bulkhead, fabricating the parachutes, developing the electronic circuitry and code, and assembling the system.

References

[1] R. James, *Aerodynamics of Recovery Systems*. New York, NY: Aerospace Press, 1999.

[2] J. Smith, "Advances in altimeter technology for high-power rocketry," *Journal of Rocketry Technology*, vol. 7, pp. 120–135, 2019.

[3] M. Williams, "Electronics advances in high-power rocketry," *International Journal of Aerospace Engineering*, vol. 10, pp. 98–107, 2005.

[4] R. Pearson, *Parachute Design and Engineering*. Los Angeles, CA: Skyrocket Publications, 2008.

[5] S. Miller, "Modern innovations in rocketry," *Journal of Advanced Rocketry*, vol. 5, pp. 50–70, 2023.

[6] Tripoli Rocketry Association, "History of the tripoli rocketry association," *Tripoli Rocketry Association Journal*, vol. 3, pp. 15–25, 2021.

[7] J. Smith, "Advances in altimeter technology for high-power rocketry," *Journal of Rocketry Technology*, vol. 7, pp. 120–135, 2019.

[8] M. Williams, "Electronics advances in high-power rocketry," *International Journal of Aerospace Engineering*, vol. 10, pp. 98–107, 2005.

[9] E. Johnson, "Integration of gps technology in modern rocketry," *Journal of Rocketry and Space Science*, vol. 12, pp. 200–215, 2020.

[10] S. Miller, "Modern innovations in rocketry," *Journal of Advanced Rocketry*, vol. 5, pp. 50–70, 2023.

[11] P. Brown, "Signal processing in bps space dual recovery systems," *Journal of High-Power Rocketry*, vol. 8, pp. 110–125, 2021.

[12] M. Green, "Avionics systems in tra high-power rockets," *Journal of Rocketry Technology*, vol. 6, pp. 80–95, 2019.

[13] R. James, *Aerodynamics of Recovery Systems*. New York, NY: Aerospace Press, 1999.

[14] R. Pearson, *Parachute Design and Engineering*. Los Angeles, CA: Skyrocket Publications, 2008.

[15] T. Venner, "Material selection for parachute fabrication," *Journal of Materials Science in Aerospace*, vol. 2, pp. 45–59, 1993.

[16] A. Knight, "Pyrotechnic charges in aerospace applications," *Aerospace Engineering Journal*, vol. 19, pp. 160–175, 1983.

[17] FreeCAD, "Rocket ejection charge calculator," 2021, accessed: 2024-08-20. [Online]. Available: https://wiki.freecad.org/Rocket_Ejection_Charge_Calculator

[18] W. Davis, "Mechanical ejection systems in model rocketry," *Journal of Mechanical Engineering*, vol. 15, pp. 200–220, 2004.

[19] D. Smith, "Enhancing safety in rocket parachute systems," *Journal of Space Safety*, vol. 29, no. 3, pp. 111–125, 2022. [Online]. Available: https://doi.org/10.1016/j.spacesafety.2022.04.002

[20] J. Anderson, "High-precision apogee detection algorithms for rocketry," *Journal of Aerospace Engineering*, vol. 55, no. 4, pp. 789–803, 2021. [Online]. Available: https://doi.org/10.1016/j.aerospace.2021.01.003

[21] E. Johnson, "Telemetry and data logging for high-power rocketeers," *Space Technology*, vol. 48, no. 1, pp. 234–245, 2020. [Online]. Available: https://doi.org/10.1016/j.spacetech.2020.07.001

[22] L. Miller, "Control systems for rocket parachute deployments," *International Journal of Rocket Science*, vol. 33, no. 2, pp. 102–115, 2019. [Online]. Available: https://doi.org/10.1016/j.ijrs.2019.05.007

[23] T. R. Association, "Advanced flight software and deployment systems," Tripoli Rocketry Association, Tech. Rep., 2021. [Online]. Available: https://www.tripoli.org/resources/flight-software-report-2021

[24] B. Space, "Telemetry system for high-power rockets," 2021, available at: https://bps.space/telemetry.

[25] T. R. Association, "Telemetry and data communication in high-power rocketry," 2020, available at: https://www.tripoli.org/telemetry.

A Appendix

A.1 Time plan

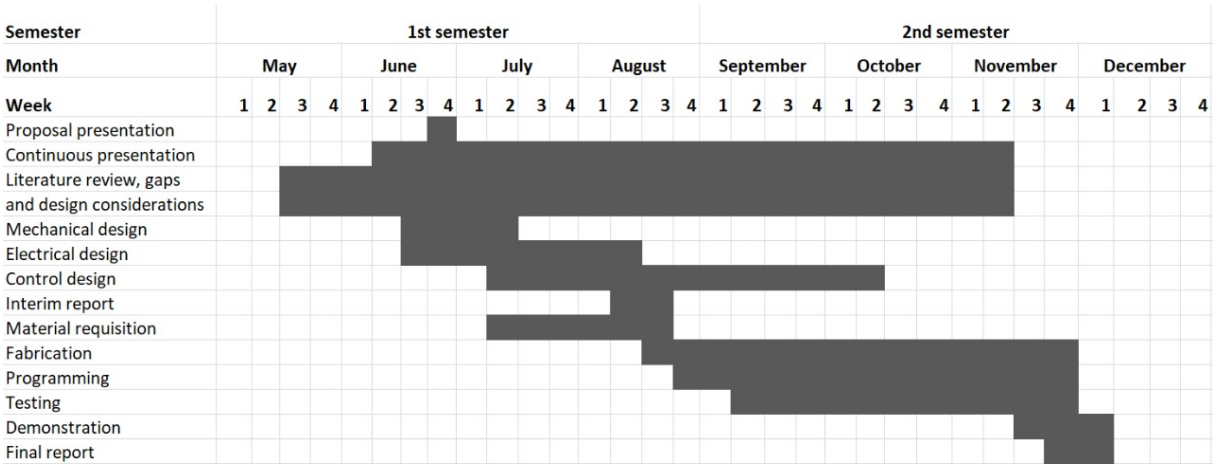

Figure A.1: Time plan

A.2 Budget

Item	**Description**	**Quantity**	**Cost per Unit (KES)**	**Total Cost (KES)**
PLA filament	1.75mm diameter	1	3000	3000
Controller	Microcontroller	1	1800	1800
Parachute Fabric	Nylon, 10m	1	2000	2000
Sensors	IMU, GPS, BMP	1	4710	4710
POM Plastic	100mm, 1m long	1	1000	1000
Pyrotechnics	Black powder	1	1600	1600
Threaded Rod	5mm diameter, 1m	1	400	400
Aluminum Rod	5mm diameter, 1m	1	400	400
Shock cord	Tubular nylon	1	2000	2000
Cells	Lithium-ion	4	500	2000
Total	-	-	-	**18910**

Table A.1: Budget

A.3 Design Drawings

Main Parachute

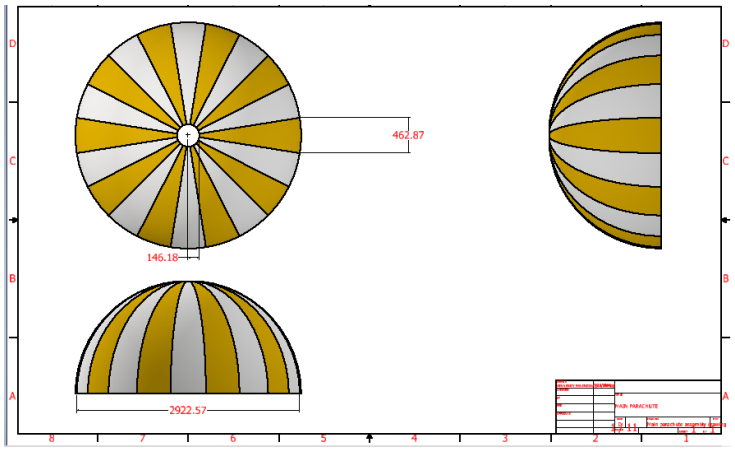

Figure A.2: main parachute

Drogue Parachute

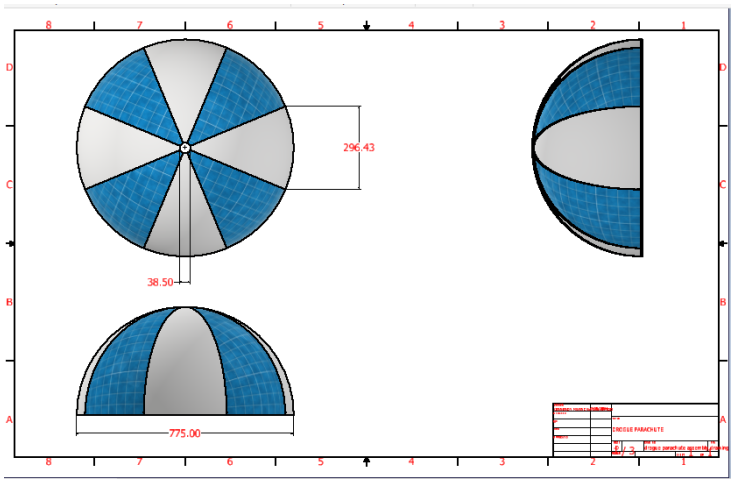

Figure A.3: drogue chute

Avionics bay sub assembly

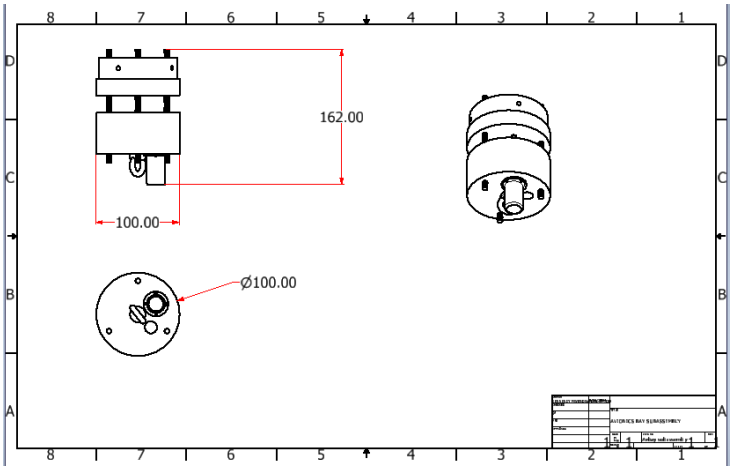

Figure A.4: avionics bay sub assembly

Avionics bay lid

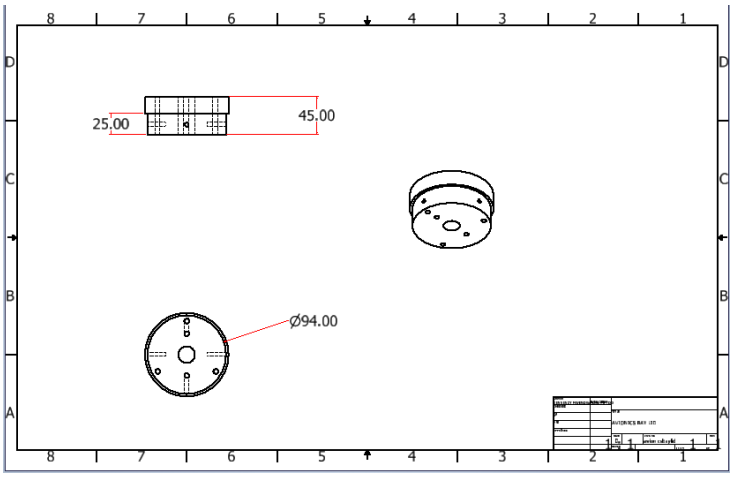

Figure A.5: avionics bay lid

Avionics bay protector

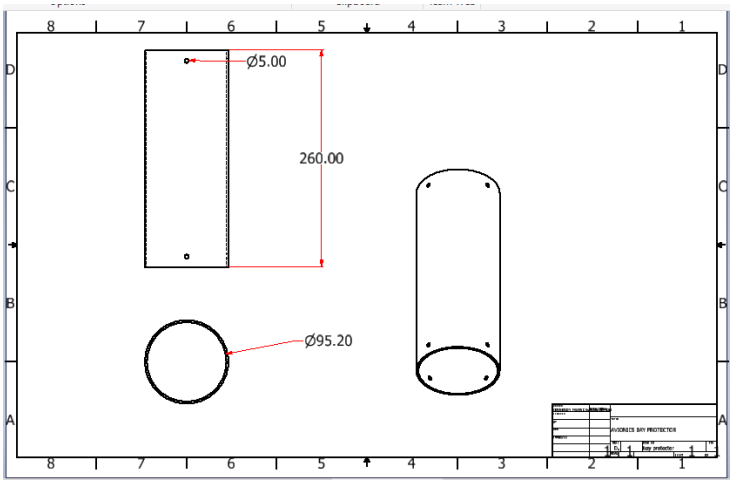

Figure A.6: avionics bay protector

Bulkhead

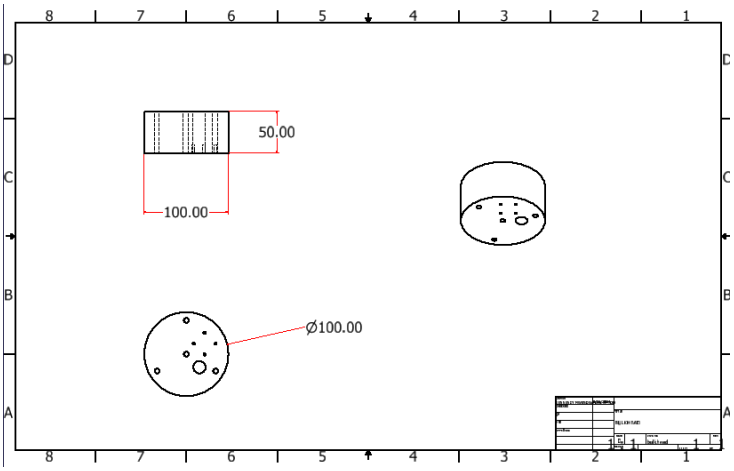

Figure A.7: bulkhead

Charge protector

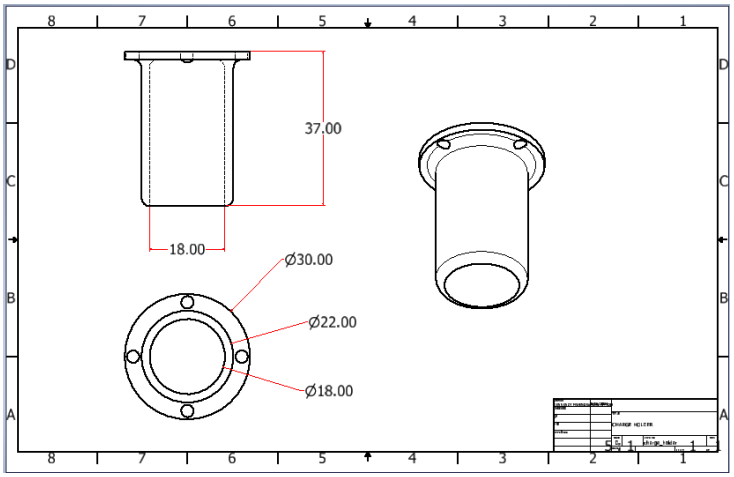

Figure A.8: charge holder

Eye bolt

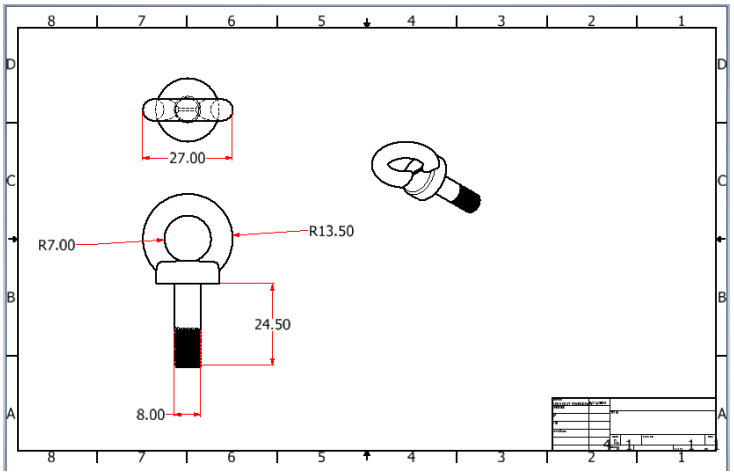

Figure A.9: eye bolt

Shear pin

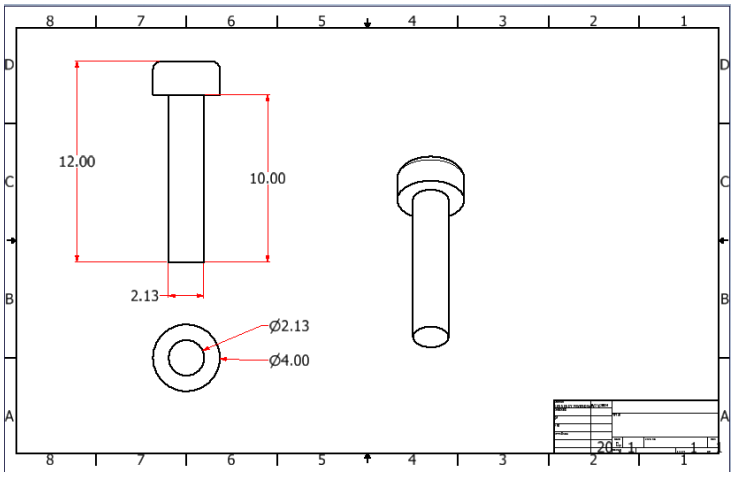

Figure A.10: shear pin

Avionics Bay Assembly

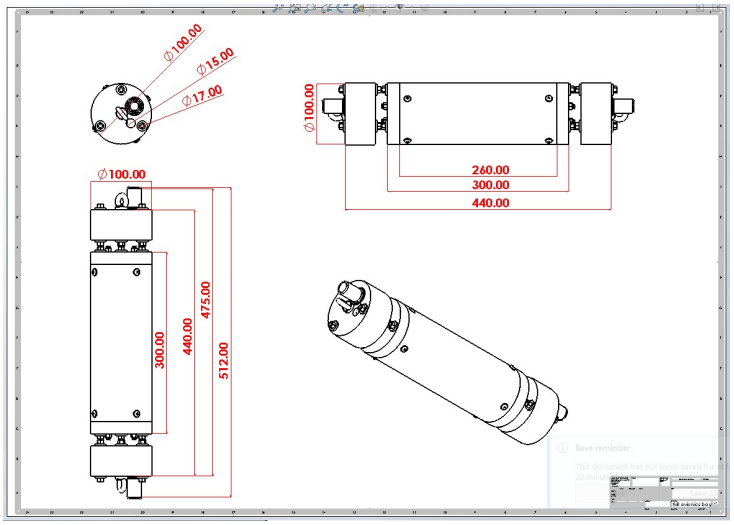

Figure A.11: Avionics Bay Assembly